



**PCMDI Report No. 49**

**COMPARISON OF THE 200 HPA CIRCULATION IN CSM  
AND CCM3 SIMULATIONS & NCEP & ERA REANALYSIS:  
PRINCIPAL AND COMMON PRINCIPAL**

by

**James S. Boyle**

**Program for Climate Model diagnosis and Intercomparison  
Lawrence Livermore National Laboratory, Livermore, CA, USA**

**October 1998**

**PROGRAM FOR CLIMATE MODEL DIAGNOSIS AND INTERCOMPARISON  
UNIVERSITY OF CALIFORNIA, LAWRENCE LIVERMORE NATIONAL LABORATORY,  
LIVERMORE, CA 94550**

#### DISCLAIMER

This document was prepared as an account of work sponsored by an agency of the United States Government. Neither the United States Government nor the University of California nor any of their employees, makes any warranty, express or implied, or assumes any legal liability or responsibility for the accuracy, completeness, or usefulness of any information, apparatus, product, or process disclosed, or represents that its use would not infringe privately owned rights. Reference herein to any specific commercial product, process, or service by trade name, trademark, manufacturer, or otherwise, does not necessarily constitute or imply its endorsement, recommendation, or favoring by the United States Government or the University of California. The views and opinions of authors expressed herein do not necessarily state or reflect those of the United States Government or the University of California, and shall not be used for advertising or product endorsement purposes.

This report has been reproduced  
directly from the best available copy.

Available to DOE and DOE contractors from the  
Office of Scientific and Technical Information  
P.O. Box 62, Oak Ridge, TN 37831  
Prices available from (615) 576-8401, FTS 626-8401

Available to the public from the  
National Technical Information Service  
U.S. Department of Commerce  
5285 Port Royal Rd.,  
Springfield, VA 22161

## Abstract

In this paper the interannual variation of monthly mean vorticity and divergence at 200 hPa are compared from four data sources: The NCEP/NCAR reanalyses 1958 through 1994, the ECMWF (ERA) reanalyses, 1979 through 1994, a NCAR CCM3 integration using prescribed SSTs from 1979 through 1993, and the NCAR CSM 300 year integration. Four twenty year periods were taken from the 300 year simulation for analysis. The NCEP, ERA and CCM3 all provide data for the period 1979 through 1993. The techniques used are principal and common principal component analyses on the fields transformed to spherical harmonics. The seasonal cycle is removed.

For the common time period, 1979 through 1993, the ERA, NCEP and CCM3 display a close correspondence in their the leading PCs of the 200 hPa vorticity. This mode is closely related to the ENSO variations of the period but the agreement extends to the extratropics. All four CSM periods have leading modes similar to each other which are dominated by a PNA type pattern and lack any Equatorial Pacific ENSO signature.

The agreement between the leading PCs for the ERA, NCEP and CCM3 for the 200 hPa divergence was somewhat less than that of the vorticity. The CCM3 and ERA indicate a somewhat larger magnitude center in the Equatorial Pacific about the dateline than NCEP. The CSM has an intense center a farther east at 150E. There are indications in the vorticity and divergence fields that this center is at the source for waves propagating to the midlatitudes yielding the PNA structures.

Two twenty year periods of the 1958 to 1996 NCEP reanalyses show a distinct difference between the two periods. The variations are comparable in magnitude if not nature to the variations seen amongst the 20 year time sections of the CSM run examined.

A CPC analysis of the NCEP, ERA and CCM3 show a common ENSO type response as the leading common component. The CCM3 model departs from the reanalyses for the second component. Combining the CCM3, CSM, NCEP and ERA shows that the CSM does share a common component ENSO related feature. Both the CSM, and CCM3 depart in the same manner with regard to the second common component which has a PNA like nature..

## Introduction

This work will present comparisons of the interannual variations of the upper level monthly mean circulations for the NCAR Climate Simulation Model (CSM, Boville and Gent, 1998) 300 year run, NCAR Community Climate Model version 3 (CCM3, Kiehl et al., 1998) AMIP simulation, and the NCEP/NCAR and ECMWF (ERA) reanalysis data sets. This work has several aims. One is to look at the available reanalyses data sets and compare them from a specific perspective. This will provide an idea of the uncertainties still inherent in our knowledge of these aspects of the contemporary atmospheric state. Another purpose is to evaluate the CCM3 and CSM simulations against the reanalyses data. Finally, this work represents an initial attempt to explore the types of variability seen in an extended coupled integration with this new system.

The analysis is carried out globally for the monthly mean windfield at 200 hPa. From the winds fields both the vorticity and divergence are computed. This upper level circulation is active in both the Tropics and midlatitudes and enables a global assessment of model performance. These variables are the significant dynamical quantities carried in the models. Over the globe the 200 hPa level is probably a fair compromise for a level of key activity. It is a bit low the Tropics and high for the polar regions. The 200 hPa level has been used often in reporting results from modeling studies, Blackmon et al. 1983 and Lau, 1985, Hoerling et al. 1992. It is also used in theoretical work involving barotropic models e. g. Branstator 1985, Held and Kang (1987). It is observed that the ENSO signal in the extratropics is quite pronounced at this level.

The AMIP, Gates(1995), protocol prescribed the time evolving observed SSTs as the boundary condition for the atmospheric models. This dictates that the AMIP integrations should share some common characteristics with the reanalyses, which presumably will have similar responses to the varying SST. For diagnosis of a coupled model the emphasis changes, from looking for a specific response to a sequence of prescribed SSTs to looking for similar type of phenomena and responses without regard to specific time sequences beyond seasonally forced variations. Thus, some of the methods used here attempt to characterize the flow in general terms, not by trying to fit any specific model or flow patterns.

Hurrel et al. (1998) and Boville and Hurrel (1998) show that the CCM3 produces a very reasonable climatology compared to the observations and that the CSM and CCM3 agree closely on most aspects of the atmospheric circulation. Meehl and Arblaster (1998) carried out a close examination of the Asian/Australian monsoon and the ENSO in this CSM integration. They show the model represents most of the major features of the monsoon system and its connections of the tropical Pacific. For a time series of the NINO-3 region they show that the CSM is producing about 60% of the amplitude of the observed variability. Further, the correlations globally with these regions reproduce the main features of the observed variations accompanying ENSO. The CSM does show its largest amplitude ENSO SST anomalies in the western tropical Pacific compared to the observed SST variability maximum in the central and eastern tropical Pacific. This paper is not intended to be a study of the ENSO events in the CSM, but by considering the dominant modes of interannual variations in the observations and models the ENSO takes center stage, at least for the observations.

In the next section the reanalyses data sets will be described, followed by a description of the model data. The following section will outline the analysis techniques. The next section will describe the Principal Component Analysis (PC) of vorticity and divergence, followed by a section with the Common Principal Component (CPC) analyses of these fields. Finally, there will be a section on conclusions.

## Data

### a. *Re-analyses*

The reanalyses data are available from two sources. The first is the NCEP/NCAR reanalyses described by Kalnay et al. (1996). These data are provided on a 2.5 x 2.5 degree longitude latitude grid and consist of monthly means from 1958 through 1996. The second set is the ECMWF Reanalysis (ERA) described by Gibson et al.(1997). These data are also on a 2.5 x 2.5 degree grid and are monthly means spanning the period form 1979 through 1993. Both the reanalyses are an attempt to eliminate the problem of changing data analysis systems which plagued the archived operational data sets. Both reanalyses ingest approximately the same observational data and the assimilation models are forced by nearly identical SSTs. Although the reanalyses have a uniform assimilation system they both suffer from a changing observational network, as stations change and as different remote sensing data are introduced. These changes in input data are convolved with the natural variability making esti-

mates of ‘true’ variability uncertain. The shortness of the data record also limits the resolution of the slower time scales.

In data sparse regions the signature of the assimilation techniques and models can make a significant contribution. The rotational wind is more closely tied to the observational data and less influenced by the idiosyncrasies of an individual assimilation system and models. The divergent wind is still subject to a large degree of uncertainty. The ERA and NCEP groups are forthright in pointing out that this field is strongly colored by the assimilation model and that the definitive description of divergence is still a goal to be achieved.

In the following work, the NCEP re-analyses data are divided into periods of varying lengths to best match the methods or verifying data. The prime period being the period 1979 to 1993 where both the ERA and NCEP reanalyses and the CCM3 simulation data are available. For comparison to the 300 year CSM integration, it is desirable to make use of the longer NCEP period, recognizing some possible inhomogeneities in the analysis.

### *b. Models*

The CSM is described by Boville and Gent (1998). The CCM3 is the atmospheric component and is described by Kiehl et al. (1998).

The CCM3 simulation data used is for the AMIP II period, 1979 through 1993. The SSTs prescribed for the CCM3 run are monthly means of the data used by the NCEP reanalysis system, using the Reynold’s SSTs after November 1982. The CSM data is from a 300 year run, Kiehl et al (1998). The CSM integration is sampled for 20 year intervals, to facilitate comparison to the reanalyses, and to assess the modes of variability in these time scales. The time sections chosen are the integrations years, 16 through 35, 36 through 55, 80 through 99, and 100 through 119. All but the first period were chosen rather arbitrarily. Where all the 20 year chunks exhibit essentially similar behavior, the 16-35 period will be used, since this is described by Meehl and Arblaster (1998).

## **Analysis techniques**

The spherical harmonic coefficients of the anomaly data were analyzed using the principal component(PC) routine PRIN from the IMSL (1990) subroutine library. A spherical truncation of T10 was applied to all the data sets. These monthly mean data

with the seasonal cycle removed were used to compute a covariance matrix for input into the PC routine. The time series length varied from thirty nine to fourteen years. The rather severe spatial truncation is the same as Hoerling et al. (1992), and is used to emphasize the large scale features and to make the computations more tractable.

The CPC technique is comprehensively described by Flury (1988). Sengupta and Boyle (1998) describe the technique for the application to atmospheric model comparison. Frankignoul et al. (1995) applied the technique to an comparison of ocean models. One of the main objectives in traditional principal component analysis is to find a coordinate system in which the representation of the say  $p$  components of a multivariate vector are uncorrelated. In the search for a **common** covariance structure it is then natural to ask if it is possible to find a coordinate system in which the  $p$  variables are uncorrelated, not only in one field but in two (or several) fields simultaneously. One advantage in using the CPC model is that one can directly compare **corresponding** principal components.

In the present study the CPC analysis was carried out using an algorithm that produced results identical to the KPRINC routine from the IMSL (1991) library. In contrast to the PCs, there is a degree of arbitrariness to the ordering of the CPCs. The PCs can be ordered on the basis of the eigenvalues of the single covariance matrix, while in the case of the CPCs there are a number of covariance matrices and the ordering need not be the same for each. In the text we will attempt to make clear the relative ordering when it is important.

The CPC techniques use the identical covariance matrices as the PC procedures. The fit that is undertaken is in the spatial (spherical harmonic) domain, thus there are up to 4 distinct time series (two reanalyses, CCM3 and CSM) of the CPC for each common vector or spatial field

## Principal components of interannual variations

### a. *Vorticity*

Figure 1 shows the respective leading PCA vectors for the 200 hPa monthly mean vorticity anomalies for the NCEP, ERA and the CCM3 simulation for the period 1979 through 1993. The patterns from the NCEP and ERA are quite similar, down to the level of many individual maxima and minima. The leading pattern of the large scale, interannual variation is consistent between the analyses of the rotational wind.

The Pacific Basin is a focus of activity, with additional patterns over North America and in the tropical Atlantic. The ENSO signature is evident in the dipole straddling the Equator in the Pacific. Overall, the CCM3 performs well compared to the reanalyses. The dipole in the Equatorial Atlantic extends too far eastward over Africa and the pattern from 30E to 150E appears weak. The CCM3 has its best correspondence in the Pacific Basin where it can be assumed that the powerful modulating signal of the prescribed SSTs forces agreement. Given that this represents just a single realization the correspondence is quite good, perhaps due to the rather strong El Nino events that occurred in this period, Kumar and Hoerling (1997).

The correlation between the leading principal components and the Southern Oscillation Index (SOI) computed by the Climate Prediction Center (CPC) exceeds 0.83 for all three data sets. The percent variance explained (PVE) by the first three PCs for all three data sets is presented in Table 1. The PVE of the leading mode is modest, ranging from 14 to 15 percent. These small values might be expected for a global field with substantial amplitude in the midlatitudes where intrinsic variation plays a major role in the variability, thus confounding the ability for any single pattern fitting all the variations. The leading PC is distinct with a sharp drop to around 7 percent for the next component. The spectrum is fairly flat for components 2 and higher.

Figure 2 shows the PC leading vector for four 20 year blocks of the CSM monthly mean 200 hPa vorticity anomaly. The patterns are all similar in shape but display a fair amount of variation in the amplitude. Figure 2a is for the years 16 to 35, the period studied by Meehl and Arblaster (1998). The 80-99 period has the largest amplitude in the PNA-like pattern arching from the North Pacific over North America. We shall term this PNA-like since the prominent maxima and minima over the Pacific and North America are in alignment with the PNA poles used by Wallace and Gutzler (1981). This work is not isolating teleconnection patterns. This North Pacific/ North America pattern is rather ubiquitous and is a internal atmospheric oscillation that can be excited by a variety of forcings, Branstator (1985), Metz (1992). Kawamura et al. (1997) noted that the spatial structure of the PNA pattern was similar for their model integrations using climatological and varying SSTs. The prominent pattern in the Pacific Basin about the Equator seen in Fig. 1, is quite weak in Fig 2, if present at all. The anomaly maximum in the Pacific just northward of the Equator is systematically farther westward in the CSM compared to the corresponding feature in the NCEP and ERA (Fig. 1a,b). The lack of the dipole straddling the Equator in the Pa-

cific, indicates that this is not an ENSO dominated pattern. A SOI was computed from the monthly mean sea level pressure fields of the CSM integrations. The correlation coefficient between this SOI and the leading principal components in Fig. 2 are 0.56, 0.36, 0.43 and 0.67. All these values are substantially below those of the corresponding computations for the NCEP, ERA and CCM3, cited above. The weaker ENSO related variations in the CSM force much less synchronization of the upper level circulation and the SOI. The pattern that then dominates is the PNA like features. The SOI has the weakest correlation to the field with the most amplitude in this structure, years 80 - 99. The SOI index for this block showed a minimum in ENSO type activity compared to the three other 20 year blocks considered. The PVE of these four CSM blocks is shown in Table 2. The values of the leading mode are generally smaller than those in Table 1. The pattern might not have a dominant ENSO component but it has a comparable PVE contribution in the CSM as ENSO is in the other data sets.

Figure 3 shows the leading PC vector for three time blocks of the NCEP reanalysis. The 1958 through 1996 period is divided into two overlapping periods 1958/77 and 77/96 to provide 20 year blocks analogous to the CSM data. The entire 58/96 period is also analyzed. Overall, the patterns are consistent between the time blocks with a definite ENSO flavor. The locations of the features appears to be robust with some variation in amplitude. The correlation for the three blocks between the SOI and this leading PC is 0.92, 0.91 and 0.85, respectively. Figure 4 shows the observed SOI for the period 1958 to 1996. There is a shift in this index in going from 58/77 to 77/96, the latter period had a mean SOI significantly less than the preceding 20 years. Trenberth (1990) identified 1976/1977 as the time of a notable interdecadal climate change in the contemporary record. The change in the SOI values in the late 70s does not markedly alter the patterns between Fig. 3a and 3b. The PVE for the leading mode in Table 3 is greater for the 77/96 block, perhaps an indication of a more prominent ENSO signal. This provides a small indication of the robustness of the patterns between decades. The CSM exhibits differences beyond the variation of this tiny sample from reanalyses.

#### *b. Divergence*

Figure 5 shows the leading PC vector of the 200 hPa divergence monthly anomaly for the NCEP, ERA reanalyses and the CCM3 simulation for the period 1979

through 1993. Broadly speaking the patterns are similar. The very close correspondence between the ERA and NCEP seen in the vorticity PC of Fig. 1, is not found in Fig. 5. The regions to the west of Central and South America and over South America exhibit some marked, qualitative differences. Generally, the ERA has a slightly greater amplitude than the NCEP. NCEP does not have focused maximum at the Equator between the Dateline and 210E seen in the ERA and CCM3. This difference between reanalyses is likely a result of the divergence being more dependent on the details of the individual assimilation systems and less on the observations than the rotational wind. The CCM3 has a prominent center at 45E on the Equator not evident in the reanalyses. The leading PC for this field is related to the ENSO variations, the correlation coefficient between the PC and SOI being 0.86, 0.68 and 0.79 for the NCEP, ERA and CCM3 data sets respectively. The anomalous center of mid-Pacific equatorial divergence is characteristic of ENSO.

The PVE for the leading three PCs are shown in Table 4. The values are somewhat larger than those for the vorticity. The SSTs have a more direct influence on the tropical divergence patterns which dominate in Fig. 5. For the leading mode the ERA has distinctly smaller values in Table 4. These data also have the smallest correlation with the SOI. Evidently the variation in the ERA is not as dominated by the ENSO variations as the other two sets. The CCM3 is especially peaked for this leading, ENSO related mode. The spectrum is flat from the third PC and higher for all the data sets.

Figure 6 shows the leading PC vector for the divergence monthly mean anomalies at 200 hPa for four CSM twenty year time periods. The center of action in the Equatorial Pacific is near 150E in the CSM, which is some 30 degrees west of the ERA position and farther west than the NCEP. Meehl and Arblaster (1998) did note that the center of ENSO activity was somewhat farther west in the CSM than the observations. The CSM has a more cellular pattern akin to the ERA, not as zonally extended as the NCEP features. Many features in Fig. 6 are consistent through all the time periods, although with variation in the amplitude. In 80/99 the maximum at 150E is tightly concentrated and the Equatorial divergence is broken to the east by convergence between 210E and 240E along the Equator. Variation over Indonesia/Maritime Continent is such that the sign varies between time periods. The center at 45E at the Equator seen in the CCM3 (Fig. 5c) is also present in Fig. 6 with some variation in amplitude. The correlations between the SOI (computed from the CSM MSLP) and

the leading PC are 0.56, 0.4, 0.5, 0.7 which are in general lower than the corresponding values of previous sets. Table 5 shows a variation in the PVE amongst the periods which at the extremes exceeds the difference between the ERA and NCEP. The lack of a strong ENSO signal evidently allows for more variation amongst the modes. Comparing the CSM vorticity patterns, Fig 2, and the divergence patterns, Fig. 6, its is suggestive that the divergence center at 150E on the Equator is the position of a wave source for a the wavetrain arching up to and over North America.

Figure 7 displays the leading PC vectors for the monthly mean divergence anomaly for the two sub-periods of the NCEP reanalyses and for the entire 39 years. The differences are perhaps not as large as those seen in the CSM but certainly not negligible. Note that 58-77 has a pattern from 150E to 270E along the Equator, that is not unlike the CSM integrations. This time period is characterized by SOI values which are less negative than the 77/96 period, see Fig. 4. The Equatorial East Pacific and South America, Central America are seen to be a region of differences between the time blocks. The correlation coefficient between the SOI and the PC for the 58/96 period is 0.7 while that of the 79/93 is 0.86. The differences in the divergence fields, Figs. 7a and 7b, are a great deal more apparent than the differences in the vorticity patterns, Figs. 3a and 3b.

## 1. CPC analyses

The PCA are useful in order to characterize each data set in its own right. In order to perform a more extensive comparison, the CPC can be used. This technique provides a way to get at an estimate of the degree of similarity of the fields. As used here, this technique fits all the data sets to a common set of spatial (as represented in spherical harmonics) principal components, however each data set retains an individual ordering of the components, and its own time series of PCs.

### a. Vorticity

Figure 8 displays the results of a CPC analysis of the NCEP, ERA and CCM3 for the 200 hPa vorticity over the common period 1979 through 1992. All three share the same leading vector shown in Fig. 8a. It has many features in common with the leading PCAs for the individual data sets, Fig. 1. The CPC analyses permits each data set to have its own ordering of the set of common vectors. The second vector for both the ERA and NCEP is shown in Fig. 8b. It could be interpreted as variations among the

major climatological vorticity centers since it has a strong similarity to the annual mean pattern of this quantity. The CCM3 does not have this vector as second but rather as its third and the second vector for the CCM3 is shown in Fig. 8c. This pattern has a dominant PNA-like feature but there is also prominent structures over Eurasia. This bears a resemblance to the leading CSM vorticity PC of Fig. 2. From Table 7, it can be seen that the differences in PVE in the second vectors is not great. However, the results are suggestive that the CCM3 contains some of the elements amplified in the CSM.

Another step is to now include a CSM field into the CPC analysis including the NCEP, ERA and CCM3. The CSM output was broken into 14 year intervals and the CPC analysis was run for these intervals. Figure 9 is representative of the results. Figure 9a is the leading vector for all four data sets, this has a pattern similar to Fig. 8a but unlike Fig. 2a-d (leading CSM PCs). This indicates that the CSM does have the variation that the other fields contain but it is not the leading mode taken by itself. It does share this type of variation in common. Beyond this mode, the models and the reanalyses diverge. Fig. 9b is the second mode for both the ERA and NCEP. Figure 9c is the second mode for the CCM3 and CSM. It can be seen that the CSM inherits the same characteristics that the CCM3 displays in Fig. 8c. It at least indicates that the CCM3 does possess the same character in this field as the CSM and thus this behavior is independent of the SST specification for the CCM3 and conversely independent of any ocean simulation idiosyncrasies of the CSM. Although visually Fig. 9 resembles the results using different CSM blocks, the PVE does show substantial variation. Comparing Table 8 and Table 9, which are the PVE for two CPC analyses using the 16/35 and 80/99 CSM time blocks respectively, it is seen that the 80/99 has a somewhat smaller PVE by the leading (ENSO?) mode. The mean ( $SOI < 0$ ) values of the SOI for this period were smaller for this period than any of the others examined, and this indicates that the PVE also declines as the ENSO type variations are smaller. Table 8 and 9 represent the extremes in the PVE of the leading mode. The ordering of the CPCs was consistent for all the CSM samples.

#### *b. Divergence*

Figure 10 shows the leading two modes for the CPC analysis of the 200 hPa monthly mean divergence anomalies of the NCEP, ERA and CCM3 data sets from 1979 through 1993. The leading mode resembles Fig. 5, the PCAs for the individual data sets. The prominent center in the equatorial midPacific has the compact charac-

ter of the ERA and CCM3 data. The ERA is the least well represented as is indicated in the PVE in Table 10. The PVE indicates a large contribution from the first two CPC's. The spectrum is rather flat from the third onward.

Figure 11 shows the leading two modes for CPC of the combined NCEP, ERA, CCM3, and one CSM 200 hPa divergence. The leading mode looks like the Fig. 5 and Fig. 10a. Interestingly, the ERA has the lowest PVE, even the CSM shares more in common than the ERA, for this CSM time slice. This might be due to the fact that the CSM and CCM3 have so much in common, more so than the NCEP and ERA for the divergence field. However, there is quite a bit of variation in the PVE from different CSM time slices. Table 12 shows that for the 80/99 time period the PVE drops substantially from the 16/35 time period. For the former period the PVE resembles the ERA. The weaker ENSO during for this CSM period makes it less like the CCM3, which has a strong ENSO signal. This does show that during its reduced ENSO periods the CSM does have a pattern which has much in common to the reanalyses.

Figure 12 shows the leading two modes of the CPC for the four 20 year periods of the CSM monthly mean divergence anomalies. Table 13 shows that there is a large variation between the blocks, compared to the NCEP sample described below (Table 14). The smallest PVE is the 80/99, which had a minimum in the mean SOI index of the four blocks examined. The largest PVE is the 16/35 period examined by Meehl and Arblaster (1998).

Figure 13 shows the CPC for the two 20 year NCEP blocks. The commonality of the two blocks is not overwhelmingly although better than the CSM periods. The two time periods have a different ENSO variation as previously discussed and shown in Fig. 4. The most egregious difference between Figs. 12a and 13a, the leading CP vectors, is in the Equatorial Pacific where the CSM has the dominant maximum at 150E and NCEP's is farther east. Given this difference this is a broad correspondence between the features in Figs. 12 and 13.

## 2. Conclusions

We have analyzed the global monthly mean anomalies of vorticity and divergence at 200 hPa for the NCEP/NCAR and ERA reanalyses, and the CCM3 and CSM integrations. The anomalies are taken with respect to the mean annual cycle for each period considered. The NCEP/NCAR reanalyses were available from 1958 through

1994, the ERA from 1979 to 1993, the CCM3 data was from a AMIP integration from 1979 to 1993 and various subperiods were taken from the CSM 300 year run. Principal component and common principal component analyses were undertaken to characterize the nature of the interannual variations on the interannual, global scale. The data were transformed to spherical harmonics and truncated at T10. The analyses were carried out in the spherical harmonic domain, and brought to gridpoints for presentation.

Some basic conclusions are:

a. *PC Analysis*

(1) For the period 1979 through 1993, the NCEP and ERA vorticity leading PCs are very similar, down to a small level of detail. Evidently, the rotational wind is accurately or at least consistently captured by the reanalyses. The divergence analysis for the same period shows qualitative differences in the PC patterns between the reanalyses. The imprint of the ENSO variations for this time period are quite evident in the leading PCs for both fields.

(2) The CCM3 AMIP run has a vorticity pattern similar to the two reanalyses, but definitely not as close as they are to each other. The divergence pattern is again different, more like the ERA than NCEP.

(3) The CSM vorticity and divergence leading patterns are distinct from both the reanalyses and the CCM3 and do not display the ENSO dominated pattern of the former, rather they display a PNA type structure in the vorticity field. The divergence center of the Equatorial Pacific activity is too far west and too strong.

(4) The analyses of the two 20 year periods of the NCEP/NCAR reanalyses of vorticity and divergence definitely shows a shift between the two periods, consistent with documented changes in the SOI time series.

b. *Common Principal Component Analyses*

(5) The CPC vorticity analyses do reveal that the CSM does contain the patterns of the ENSO dominated variations in the reanalyses, but they are not the leading modes taken as themselves as in the PC results. The CSM PC analyses may look disastrously incorrect, but the CPC indicates that it does much correct and that future improvements to the Equatorial Ocean circulation should yield marked improvement.

(6) There are characteristics of the CCM3 which differs from the reanalyses which are amplified in the CSM run. The CCM3 and CSM tend to have more in com-

mon with each other than either has with the reanalyses.

General:

(7) There is a problem with defining the divergence field unambiguously from reanalyses. The divergence patterns are all quite different leading to similar vorticity patterns.

*Acknowledgments.* The generosity of the NCAR CSM modeling group in making their data available is greatly appreciated. Special thanks to Maurice Blackmon and Dennis Shea of NCAR for facilitating access to the data. This work was performed under the auspices of the Department of Energy Environmental Sciences Division by the Lawrence Livermore National Laboratory under contract W-7405-ENG-48.

References:

- Blackmon, M. L., J. E. Geisler, and E. J. Pitcher, 1983: A general circulation model study of January climate anomaly patterns associated with interannual variation of equatorial Pacific sea surface temperatures. *J. Atmos. Sci.*, **40**, 1410-1425.
- Boville, B. A., and P. R. Gent, 1998: The NCAR Climate System Model, Version One., *J. Climate*, **11**, 1115-1130.
- Boville, B. A., and J. W. Hurrel, 1998: A comparison of the atmospheric circulations simulated by the CCM3 and CSM1., *J. Climate*, **11**, 1327-1341.
- Branstator, G., 1985: Analysis of general circulation model sea surface temperature anomaly experiments using a linear model. Part II: Eigenanalysis., *J. Atmos. Sci.*, **42**, 2242-2254.
- Flury, B., 1988: *Common Principal Components and Realted Multivariate Models.*, J. Wiley, New York, pp 258.
- Frankigoul, C., S. Fevrier, N. Sennechael, J. Verbeek, and P. Braconnot, 1995: An intercomparison between four tropical ocean models: Thermocline variability. *Tellus*, **47A**, 351-364.
- Gates, W. L., 1992: AMIP: The atmospheric model intercomparison project., *Bull. Amer. Meteor. Soc.*, **73**, 1962-1970.
- Gibson, J. K., P. Kallberg, S. Uppla, A. Hernandez, A. Nomura, and E. Serrano, 1997: ECMWF Re-Analysis Project Report Series. 1. ERA Description. 66p.
- Held, I. M., and I.-S. Kang, 1987: Barotropic models of the extratropical response to El Niño. *J. Atmos. Sci.*, **44**, 3576-3586.
- Hoerling, M. P., M. L. Blackmon, and M. Ting, 1992: Simulating the atmospheric response to the 1985-87 El Niño cycle. *J. Clim.*, **5**, 669-682.
- Hoerling, M. P, L. L. Dehaan and J. W. Hurrel, 1993: Diagnosis and Sensitivity of the 200 hPa circulation in NCAR community climate models., NCAR Technical Note, NCAR/TN-394+STR, National Center for Atmospheric Research, Boulder, CO, 68 pp.
- Hurrel, J. W., J. J. Hack, D. P. Baumhefner, 1993: Comparision of NCAR community Climate Model (CCM) Climates., NCAR Technical Note, NCAR/TN-395+STR, National Center for Atmospheric Research, Boulder, CO, 335pp.
- Hurrel, J. W. , J. J. Hack, B. A. Boville, D. L. Williamson, and J. T. Kiehl, 1998: The dynamical simulation of the NCAR Community Climate Model Version 3 (CCM3). *J. Climate*, **11**, 1207-1236.

- IMSL Stat/Library, 1991: IMSL Inc., Houston, 1578pp.
- Kalnay, E. M., M. Kaniniti, R. Kistler, W. Collins, D. Deaven, L. Gandin, M. Iredell, S. Saha, G. White, J. Woolen, Y. Zhu, M. Chelliah, W. Ebisuzaki, W. Higgins, J. Janowiak, K. C. Mo, C. Ropelewski, J. Wang, A. Leetma, R. Reynolds, R. Jenne and D. Joseph, 1996: The NCEP/NCAR 40-year reanalysis project. *Bull. Amer. Met. Soc.*, **77**, 437-471.
- Kawamura, R. M. Sugi and N. Sato, 1995: Interdecadal and interannual variability in the northern extratropical circulation simulated with the JMA global model. Part I: Wintertime leading mode. *J. Clim.*, **8**, 3006-3019.
- Kiehl, J. T., J.J. Hack, G. B. Bonan, B.A. Boville, D. L. Williamson, and P. J. Rasch, 1998: The National Center for Atmospheric Research Community Climate Model: CCM3., *J. Climate*, **11**, 1131-1149.
- Kumar, A., and M. P. Hoerling, 1997: Interpretation and implications of the observed inter-El Niño variability., *J. Clim.*, **10**, 83-91.
- Lau, N.-C., 1985: Modeling the seasonal dependence of the atmospheric response to observed El Niños in 1962-1976., *Mon. Wea. Rev.*, **113**, 1970-1996.
- Meehl, G. A. and J. M. Arblaster, 1998: The Asian-Australian Monsoon and El Niño Southern Oscillation in the NCAR Climate System Model. *J. Clim*, **11**, 1356-1385.
- Metz, W., 1994: singular modes and low-frequency atmospheric variability., *J. Atmos. Sci.*, **51**, 1740-1753.
- Sengupta, S. and J. Boyle, 1998: Using common principal components for comparing GCM simulations., *J. Clim.*, **11**, 816-830.
- Simmons, A. J., J. M. Wallace, and G. W. Branstator, 1983: Barotropic wave propagation and instability, and atmospheric teleconnection patterns. *J. Atmos. Sci.*, **40**, 1363-1392.
- Trenberth, K. E., 1984: Signal Versus Noise in the Southern Oscillation, *Mon. Wea. Rev.*, **112**, 326-332.
- Trenberth, K. E., 1990: Recent observed interdecadal climate changes in the Northern Hemisphere., *Bull. Amer. Meteor. Soc.*, **71**, 988-993.
- Trenberth, K. E., 1995: Atmospheric circulation changes. *Clim. Change*, **31**, 427-453.
- Wang, B., 1995: Interdecadal changed in El Niño onset in the last four decades. *J. Clim.*, **8**, 267-285.
- Wallace, J. M. and D. S. Gutzler, 1981: Teleconnection in the geopotential height field

during the northern hemisphere winter, *Mon. Wea. Rev.*, **109**, 784-812.  
Zhang, Y., J. M. Wallace and D. S. Battisti, 1997: ENSO-like interdecadal variability:1900-93, *J. Clim*, **10**, 1004-1020.

**Table 1: Percent variance explained by PCA of 200 hpa vorticity**

Data set	1st	2nd	3rd
NCEP	13	6	5
ERA	13	7	5
CCM3	14	7	6

**Table 2: Percent variance explained for 200 hp vorticity**

CSM block	1st	2nd	3rd
16-35	13	7	5
36-55	10	7	5
80-99	10	7	5
100-119	10	7	5

**Table 3: percent variance explained for 3 time frames of NCEP reanalyses 200 hPa vorticity**

NCEP block	1st	2nd	3rd
58-77	11	7	5
77-96	13	6	5
58-96	12	7	5

**Table 4: percent variance explained for first three principal components of the 200 hPa divergence**

Data Set	1st	2nd	3rd
NCEP	44	23	9
ERA	38	25	10
CCM3	46	18	7

**Table 5: Percent variance explained for 200 hPa divergence for 4 CSM blocks**

CSM block	1st	2nd	3rd
16-35	48	17	5
36-55	42	19	7
80-99	38	21	7
100 - 119	40	20	7

**Table 6: Percent variance explained of 3 time frames of NCEP reanalyses 200 hPa divergence**

NCEP block	1st	2nd	3rd
58-77	37	25	13
77-96	41	24	10
58-96	37	26	11

**Table 7: percent variance explained leading 3 CPC for 200 hPa vorticity for the NCEP and ERA reanalyses and CCM3 simulation 1979 through 1992. The ordering is based on the NCEP eigenvalues.**

Data set	cpc 1	cpc 2	cpc 3
NCEP	14	7	5
CCM3	13*	5	7
ERA	13*	7	5

**Table 8: Percent variance explained leading 3 cpc for 200 hPa vorticity for NCEP and ERA reanalysis, CCM3 for 1979 through 1992 and a 14 year. block of CSM. The ordering is based on the NCEP eigenvalues.**

Data Set	cpc 1	cpc 2	cpc 3
NCEP	14*	7	5
CCM3	13*	5	6
ERA	12*	7	5
CSM 16 - 35	13*	4	6

**Table 9: Percent variance explained leading 3 cpc for 200 hPa vorticity for NCEP and ERA reanalysis, CCM3 for 1979 to 1992 and a 14 year. block of CSM. The ordering is based on the NCEP eigenvalues.**

Data Set	cpc 1	cpc 2	cpc 3
NCEP	14*	7	5
CCM3	13*	5	7
ERA	13*	7	5
CSM 80 - 99	7*	4	6

**Table 10: percent variance explained leading 3 CPC for 200 hPa divergence for the NCEP and ERA reanalyses and CCM3 simulation 1979 to 1992. The ordering is based on the NCEP eigenvalues.**

Data set	cpc 1	cpc 2	cpc 3
NCEP	44	22	3
CCM3	45	18	7
ERA	34	28	11

**Table 11: Percent variance explained leading 3 cpc for 200 hPa divergence for NCEP and ERA reanalysis, CCM3 for 1979 to 1992 and a 14 year. block of CSM. The ordering is based on the NCEP eigenvalues.**

Data Set	cpc 1	cpc 2	cpc 3
NCEP	43	22	10
CCM3	45	17	8
ERA	33	28	12
CSM 16-35	50	15	5

**Table 12: Percent variance explained leading 3 cpc for 200 hPa divergence for NCEP and ERA reanalysis, CCM3 for 1979 to 1992 and a 14 year. block of CSM. The ordering is based on the NCEP eigenvalues.**

Data Set	cpc 1	cpc 2	cpc 3
NCEP	40	22	9
CCM3	45	17	8
ERA	33	27	12
CSM 80-99	34	23	6

**Table 13: Percent variance explained for leading 3 CPC of 200 hPa divergence for four 20 year blocks of CSM simulation. The ordering is based on the 16-35 data eigenvalues.**

Data set	cpc 1	cpc 2	cpc 3
CSM 16 - 35	48	16	5
CSM 36 - 55	42	19	7
CSM 80-99	35	22	7
CSM 100 - 119	40	19	7

**Table 14: Percent variance explained for leading 3 CPC of 200 hPa divergence for two 20 year blocks of NCEP reanalysis. The ordering is based on the 77/96 data eigenvalues.**

Data set	cpc 1	cpc 2	cpc 3
NCEP 77/96	40	24	9
NCEP 58/77	33	28	9

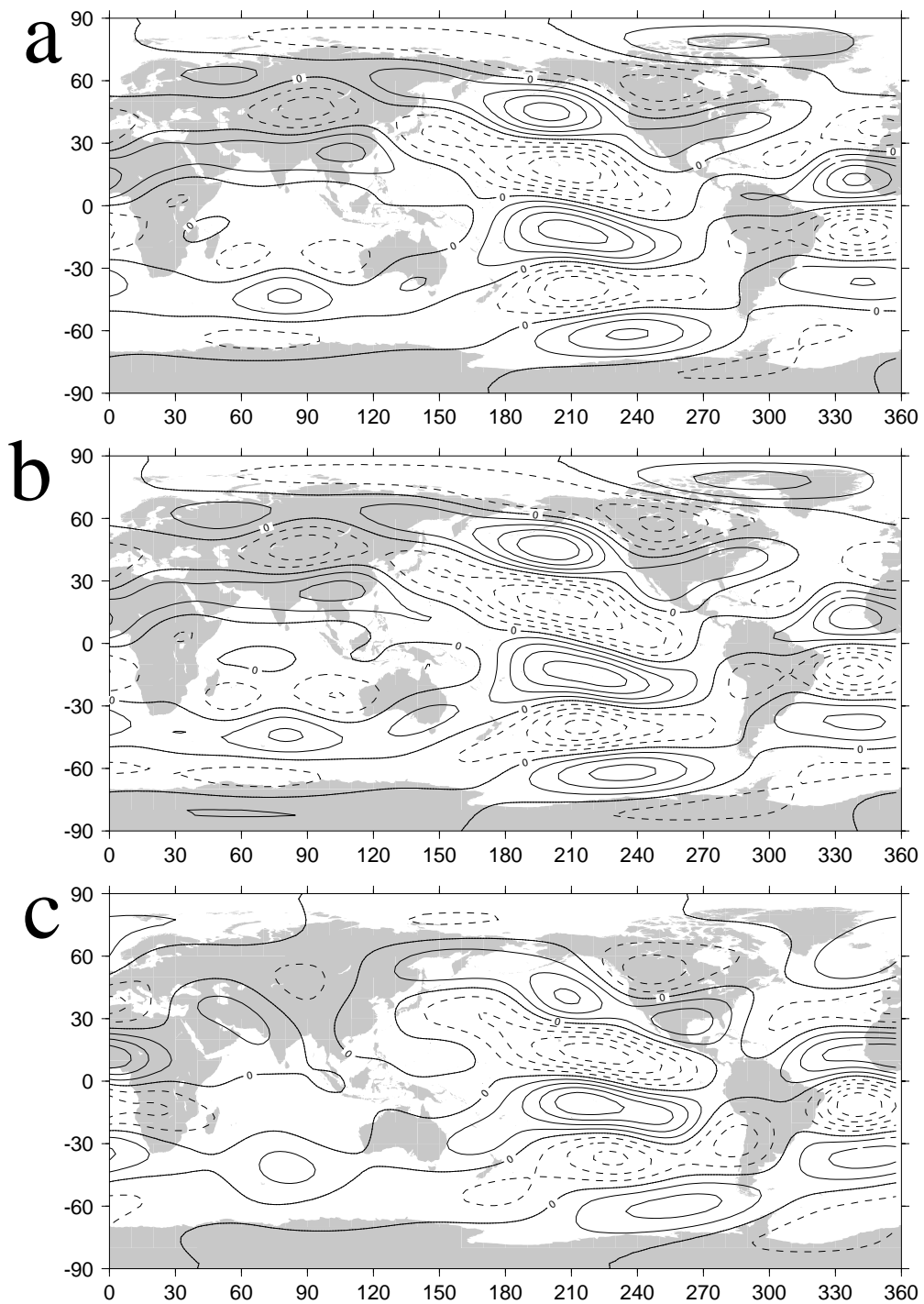


Figure 1.

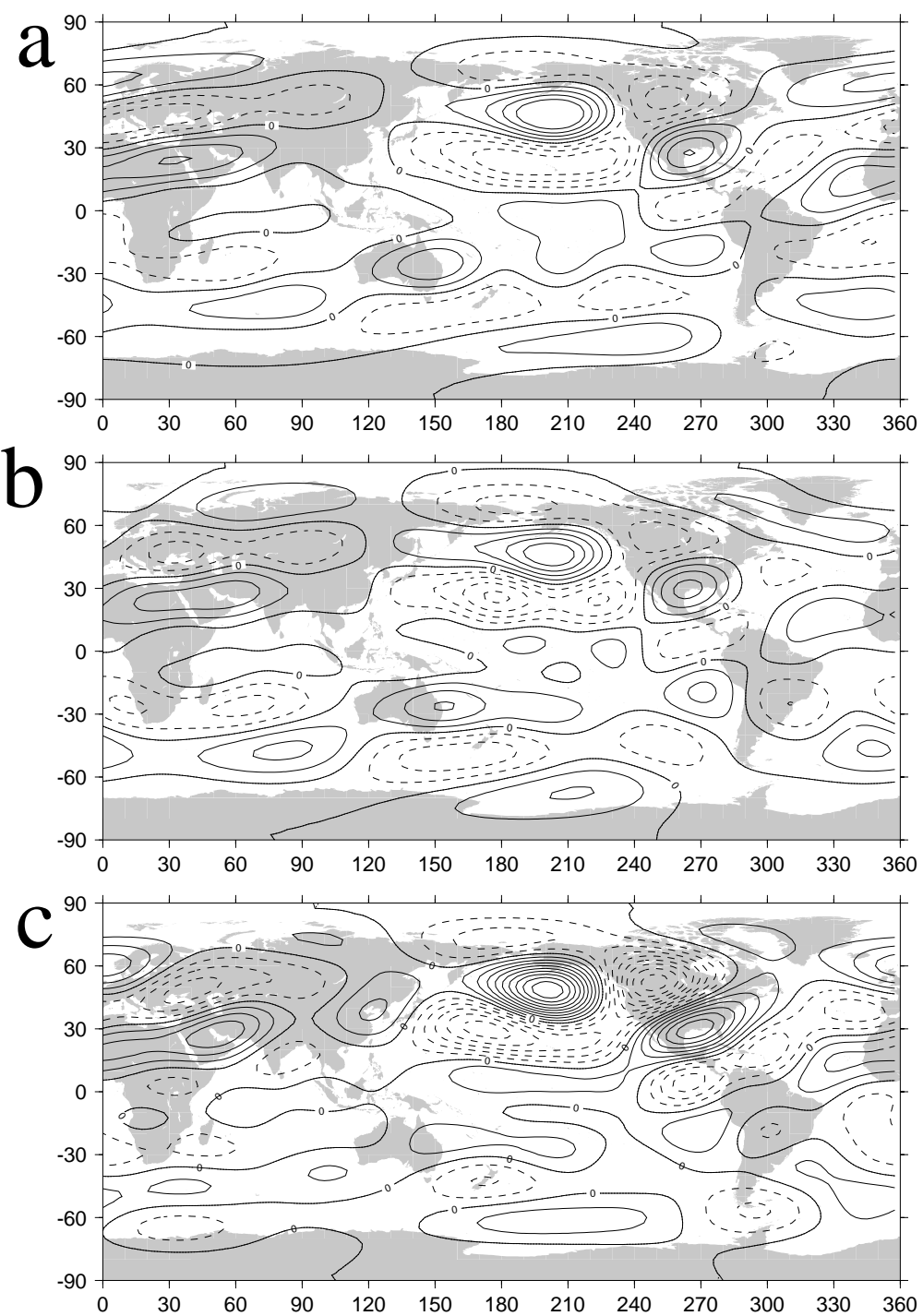


Figure 2.

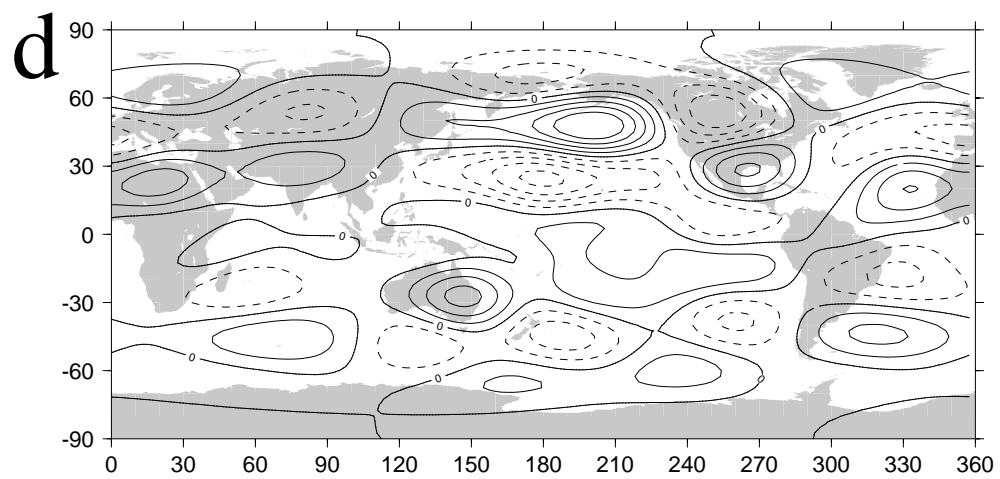


Figure 2 (con't).

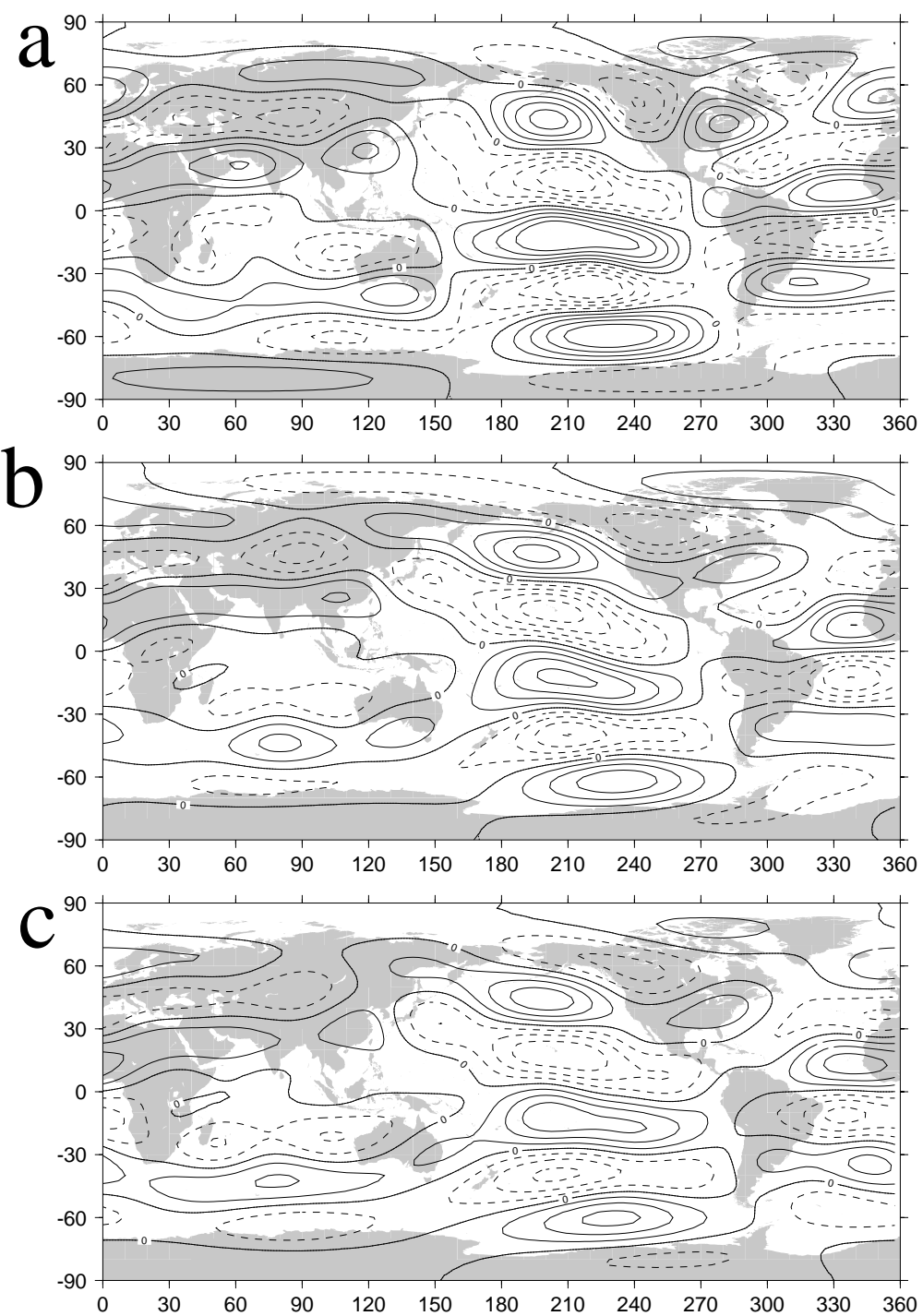


Figure 3.

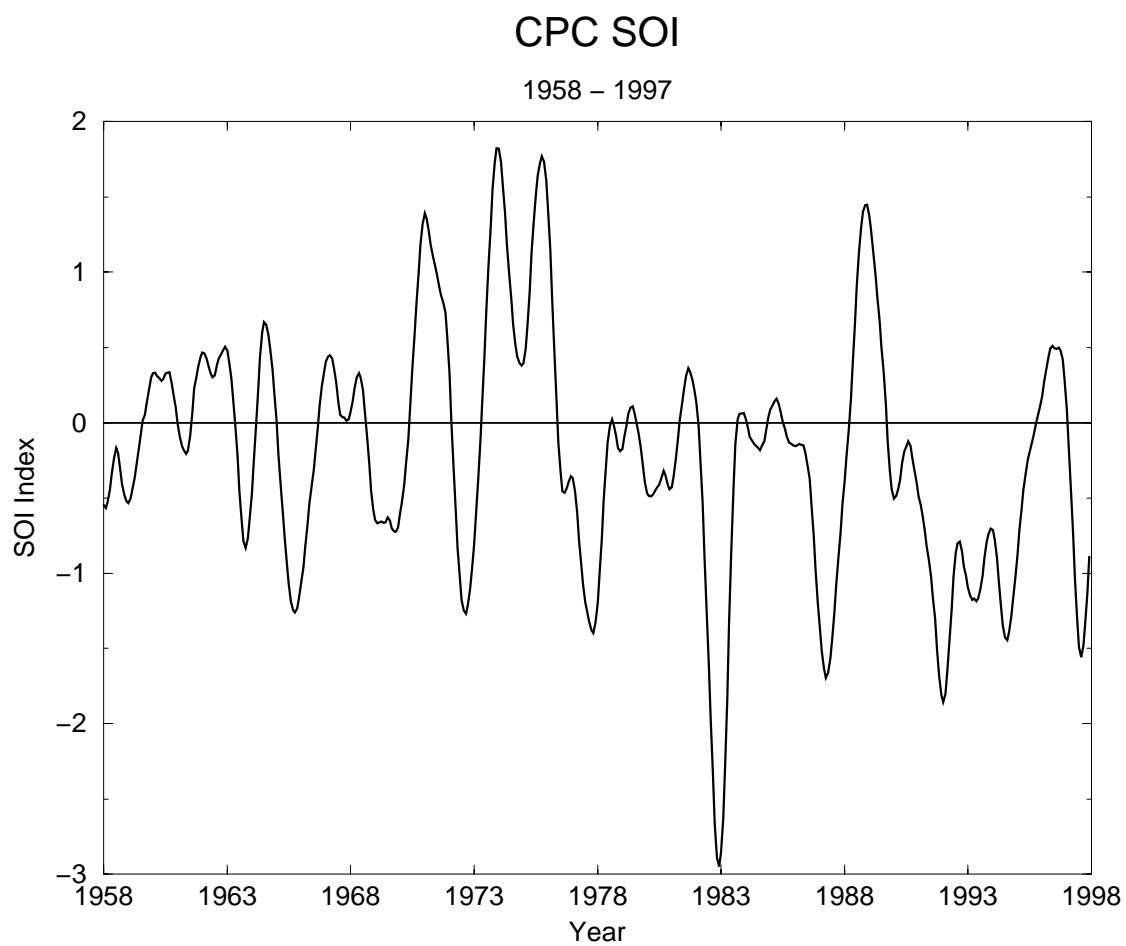


Figure 4.

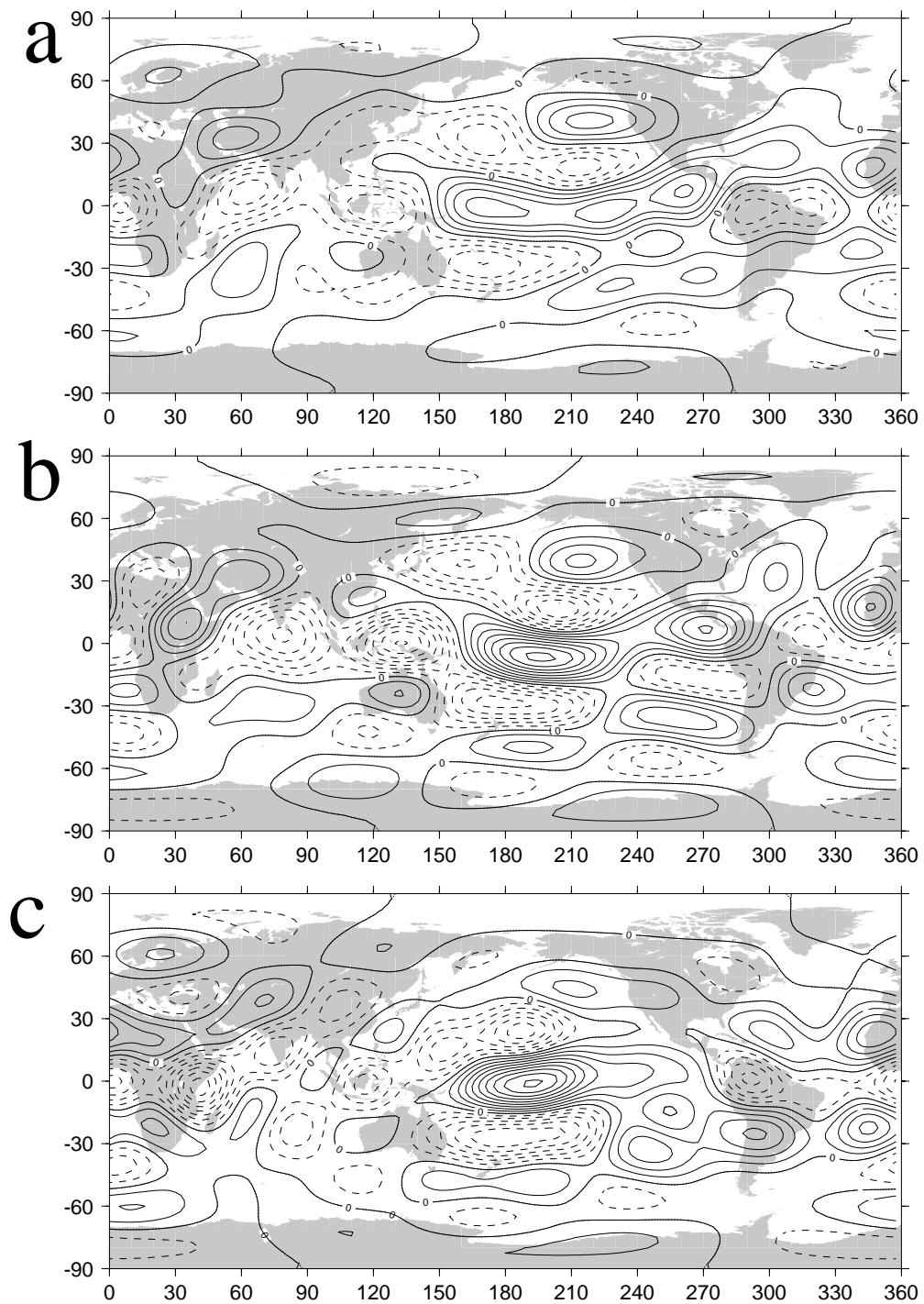


Figure 5.

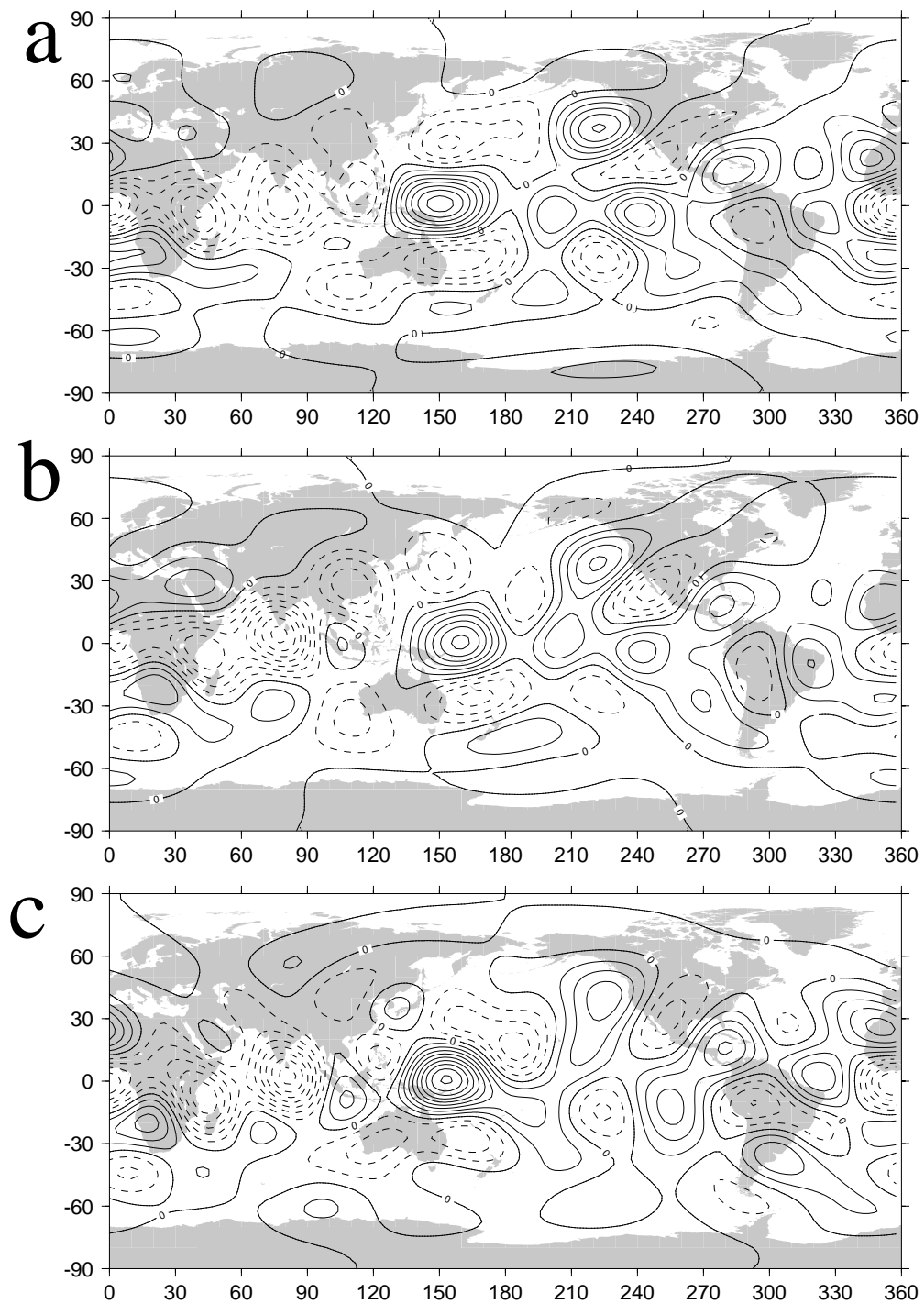


Figure 6.

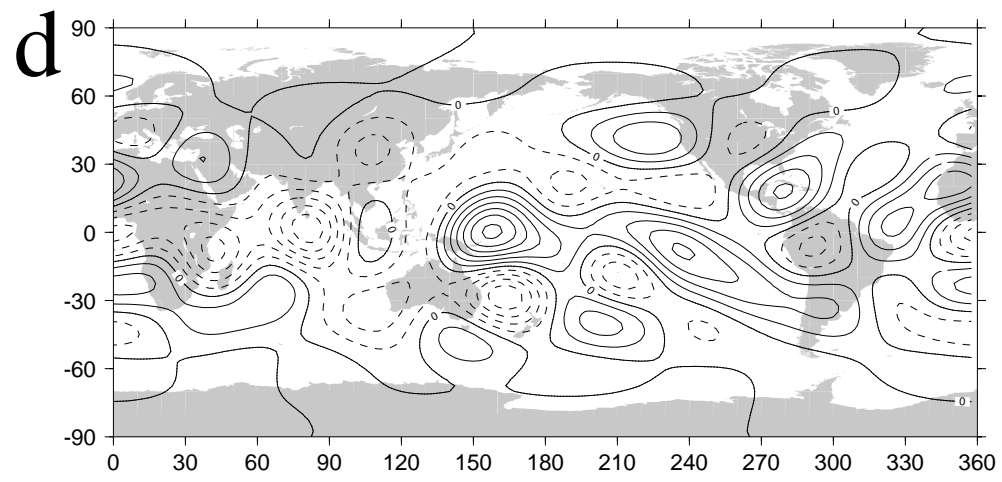


Figure 6 (cont'd).

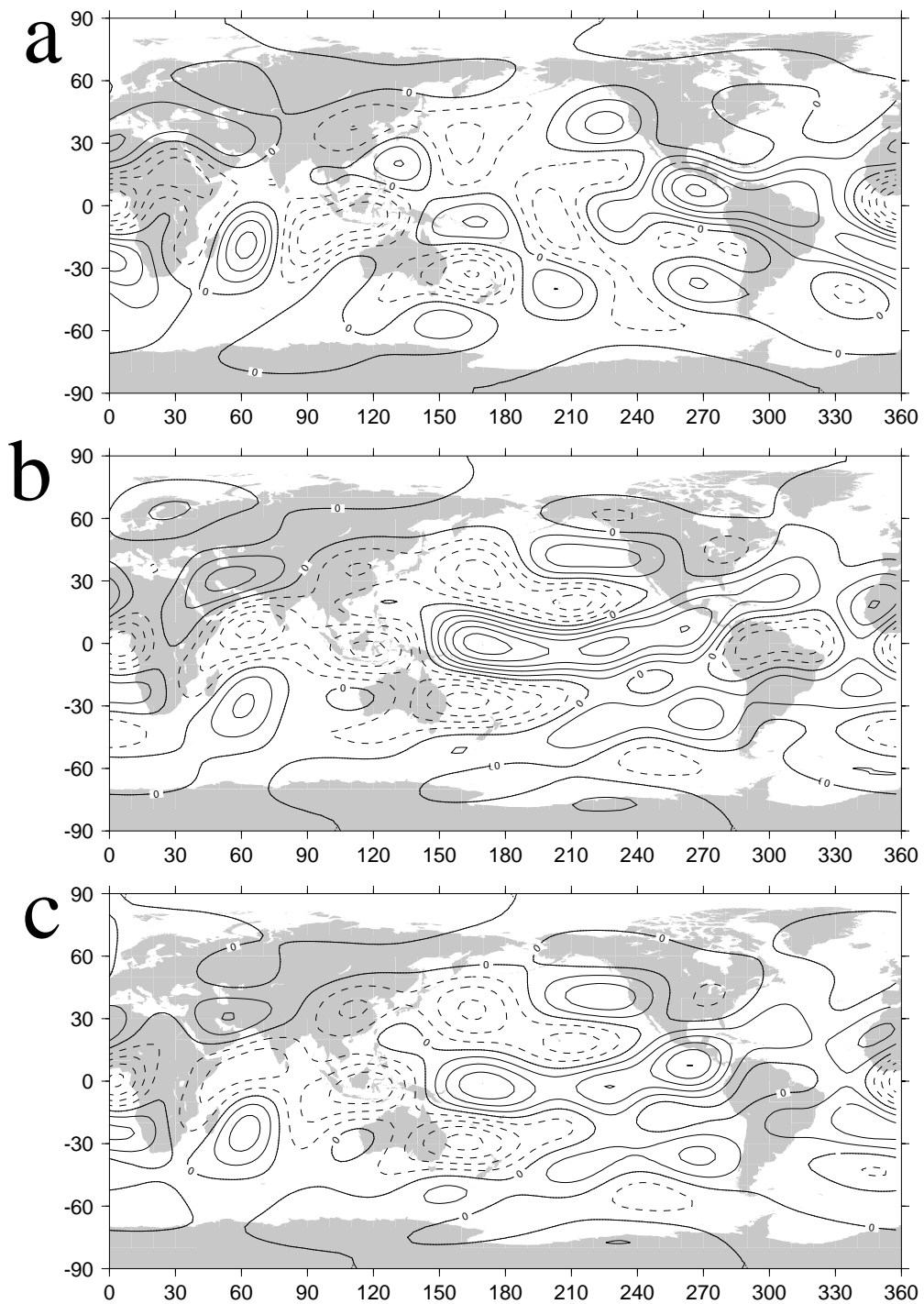


Figure 7.

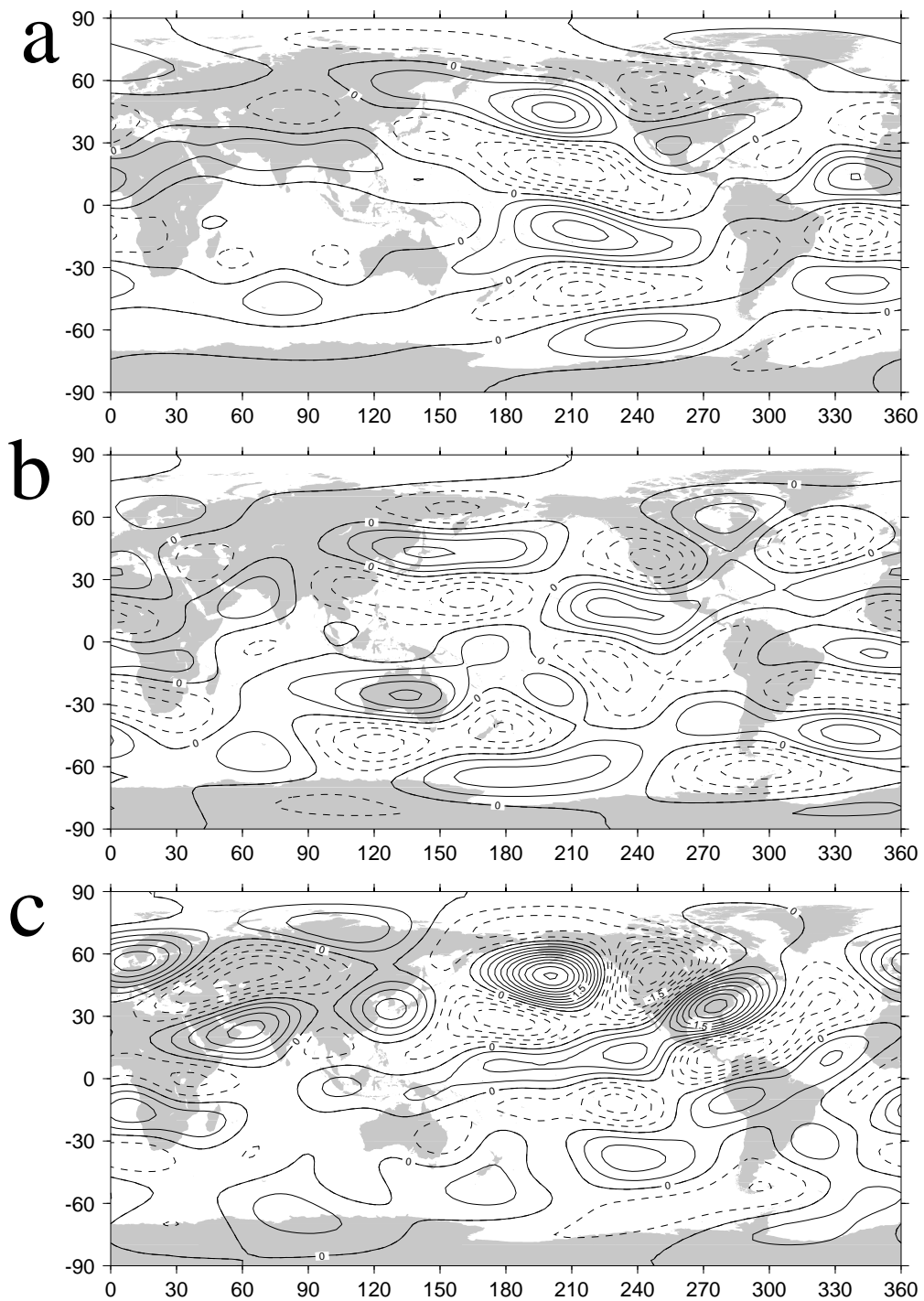


Figure 8.

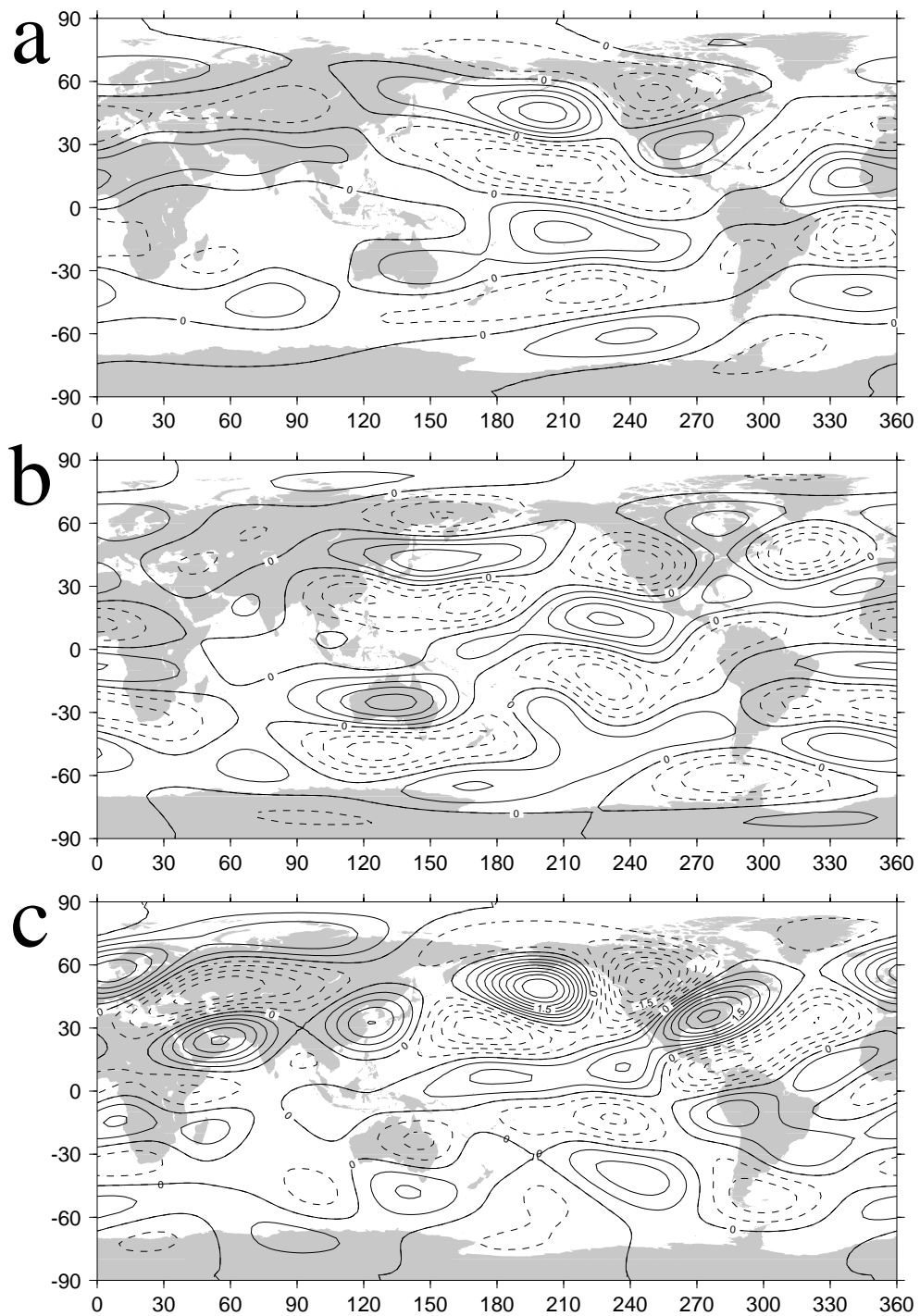


figure 9

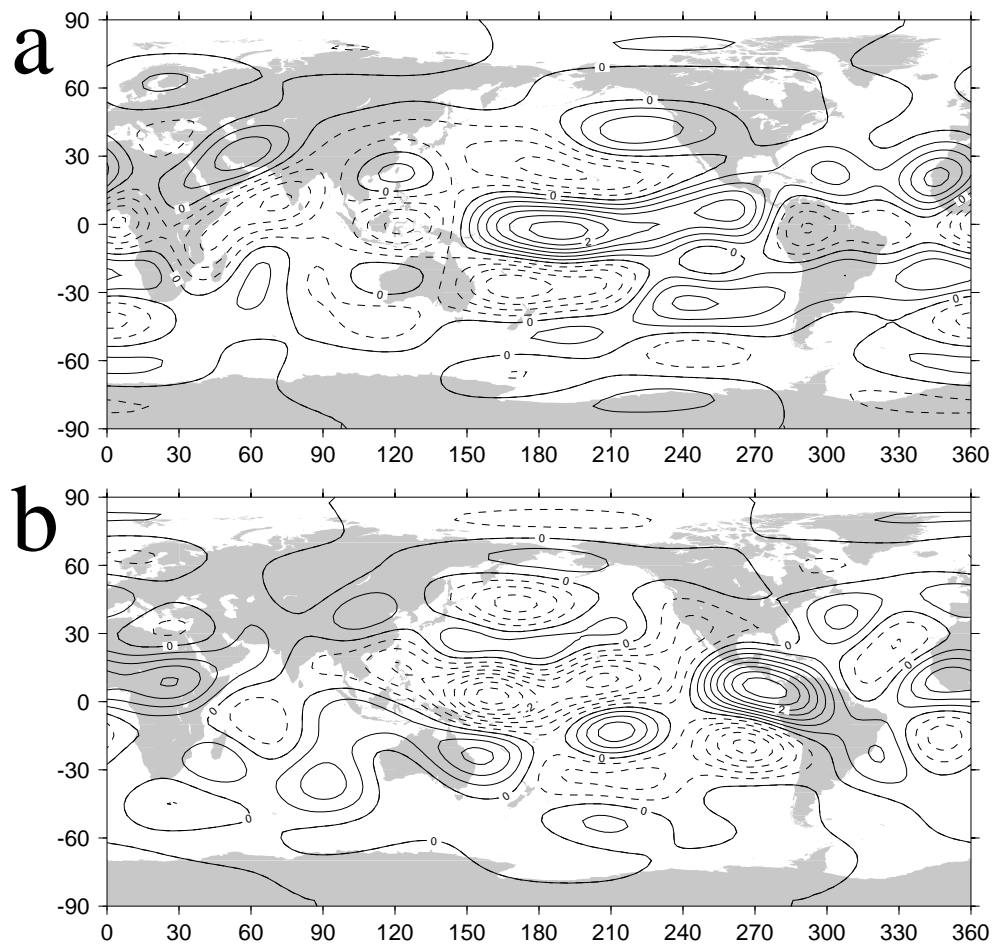


Figure 10.

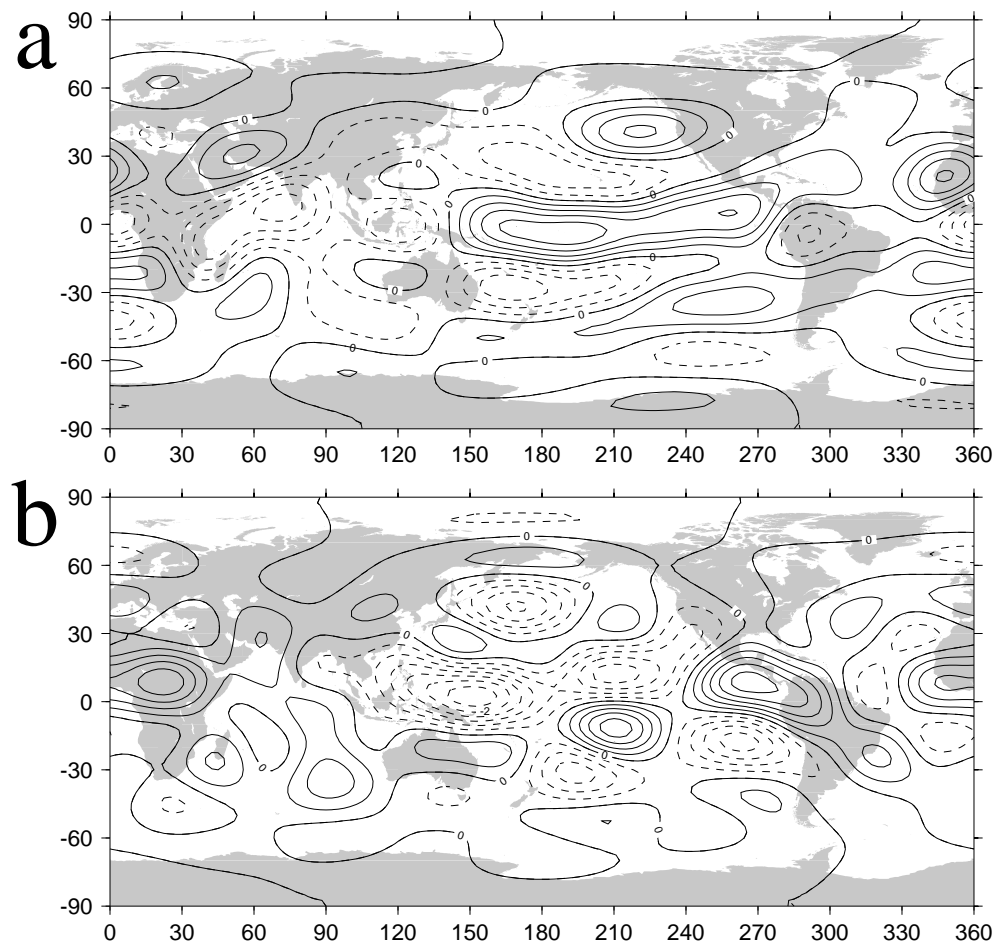


Figure 11.

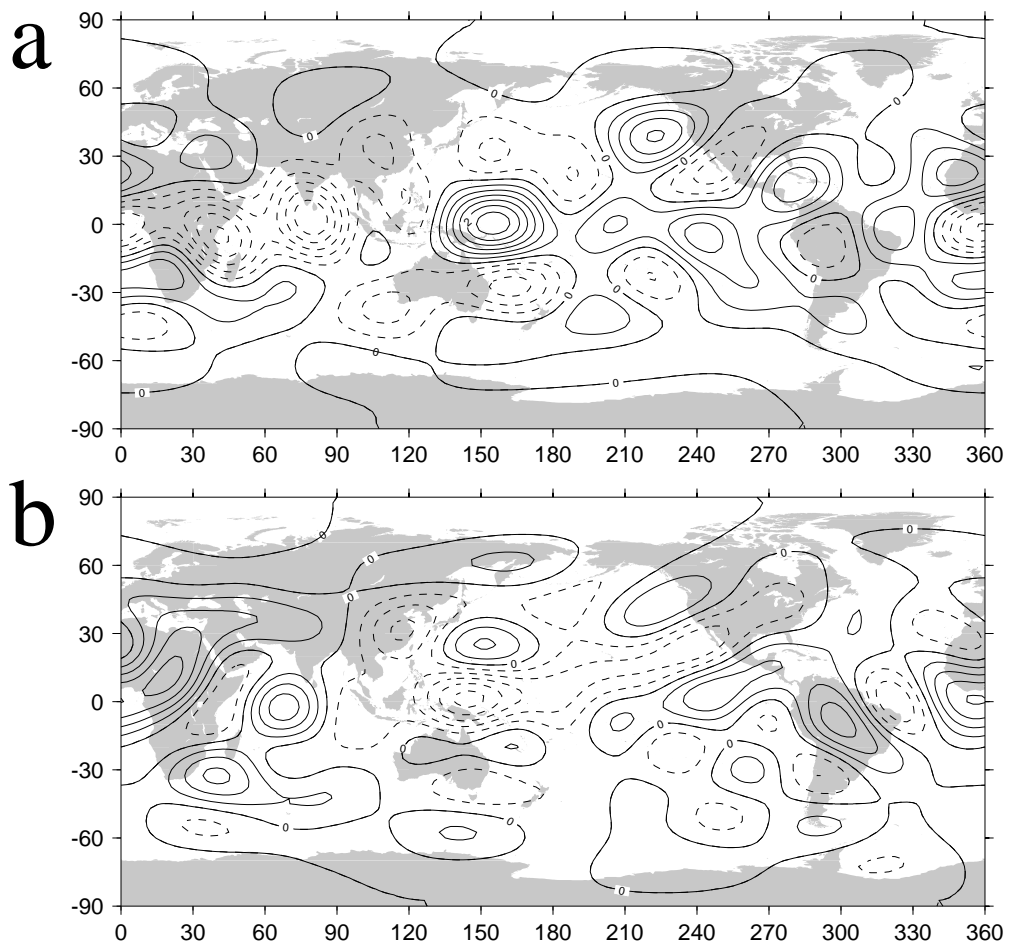


Figure 12.

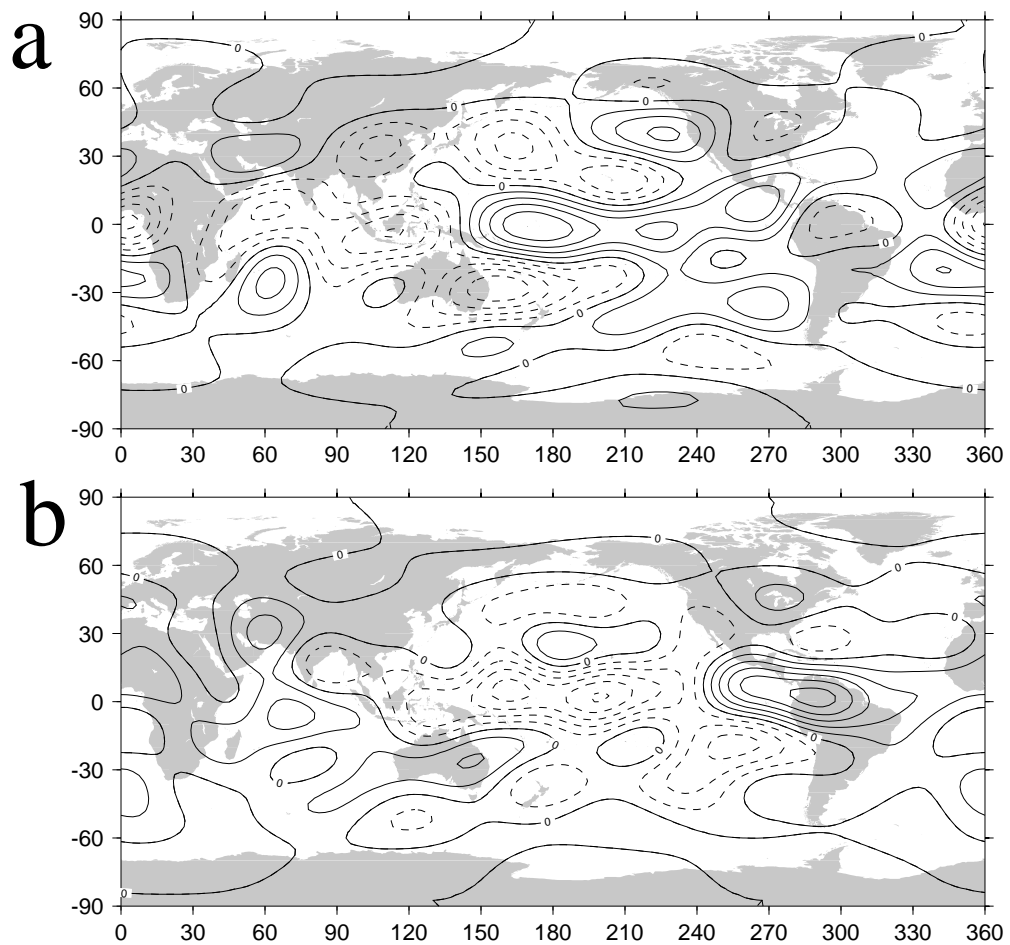


Figure 13.

## Figure Captions

- Figure 1.(a) Leading principal vector for the 200 hPa monthly mean vorticity for the NCEP/NCAR reanalyses data set for the period 1979 through 1993. Contour interval is  $1.0 \times 10^{-6} \text{ sec}^{-1}$ . Positive contours are solid, negative contours are dashed. Zero contour is annotated and is solid.  
(b) As in (a) except for the ERA data.  
(c) As in (a) except for the CCM3.

- Figure 2. (a) Leading principal vector for the 200 hPa monthly mean vorticity for the CSM data set for the integration years 16 through 35.. Contour interval is  $1.0 \times 10^{-6} \text{ sec}^{-1}$ . Positive contours are solid, negative contours are dashed. Zero contour is annotated and is solid.  
(b) As in (a) except for the integration years 36 through 55.  
(b) As in (a) except for the integration years 80 through 99.  
(b) As in (a) except for the integration years 100 through 119

- Figure 3. (a) Leading principal vector for the 200 hPa monthly mean vorticity for the NCEP/NCAR reanalyses data set for the period 1958 through 1977 . Contour interval is  $1.0 \times 10^{-6} \text{ sec}^{-1}$ . Positive contours are solid, negative contours are dashed. Zero contour is annotated and is solid.  
(b) As in (a) except for the period 1977 through 1996  
(b) As in (a) except for the period 1958 through 1996

Figure 4. A time series of the Southern Oscillation Index computed by the Climate Prediction Center for the period 1958 to 1996.

- Figure 5. .(a) Leading principal vector for the 200 hPa monthly mean divergence for the NCEP/NCAR reanalyses data set for the period 1979 through 1993. Contour interval is  $1.0 \times 10^{-5} \text{ sec}^{-1}$ . Positive contours are solid, negative contours are dashed. Zero contour is annotated and is solid.  
(b) As in (a) except for the ERA data.  
(c) As in (a) except for the CCM3.

- Figure 6. (a) Leading principal vector for the 200 hPa monthly mean divergence for the CSM data set for the integration years 16 through 35.. Contour interval is  $1.0 \times 10^{-5} \text{ sec}^{-1}$ . Positive contours are solid, negative contours are dashed. Zero contour is annotated and is solid.  
(b) As in (a) except for the integration years 36 through 55.  
(b) As in (a) except for the integration years 80 through 99.  
(b) As in (a) except for the integration years 100 through 119

Figure 7. (a) Leading principal vector for the 200 hPa monthly mean divergence for the NCEP/NCAR reanalyses data set for the period 1958 through 1977. Contour interval is  $1.0 \times 10^{-5} \text{ sec}^{-1}$ . Positive contours are solid, negative contours are dashed. Zero contour is annotated and is solid.

(b) As in (a) except for the period 1977 through 1996

(b) As in (a) except for the period 1958 through 1996

Figure 8. Common Principal vectors for the 200 hPa monthly mean vorticity for the NCEP/NCAR, ERA reanalyses and the CCM3 data sets for the period 1979 through 1993. Contour interval is  $1.0 \times 10^{-6} \text{ sec}^{-1}$ . Positive contours are solid, negative contours are dashed. Zero contour is annotated and is solid.

(a) Leading CPC vector for all three data sets.

(b) The second CPC vector for the NCEP and ERA renalyses.

(c) The second CPC vector for the CCM3.

Figure 9. Common Principal vectors for the 200 hPa monthly mean vorticity for the NCEP/NCAR, ERA reanalyses, the CCM3 and CSM(16-35) data sets for a 14 year period. . Contour interval is  $1.0 \times 10^{-6} \text{ sec}^{-1}$ . Positive contours are solid, negative contours are dashed. Zero contour is annotated and is solid.

(a) Leading CPC vector for all four data sets.

(b) The second CPC vector for the NCEP and ERA renalyses.

(c) The second CPC vector for the CCM3.

Figure 10. Common Principal vectors for the 200 hPa monthly mean divergence for the NCEP/NCAR, ERA reanalyses and the CCM3 data sets for the period 1979 through 1993. Contour interval is  $1.0 \times 10^{-6} \text{ sec}^{-1}$ . Positive contours are solid, negative contours are dashed. Zero contour is annotated and is solid.

(a) The leading CPC vector for all the data sets.

(b) The second CPC vector for all the data sets.

Figure 11. Common Principal vectors for the 200 hPa monthly mean divergence for the NCEP/NCAR, ERA reanalyses, the CCM3 and one CSM data set for 14 year periods.. Contour interval is  $1.0 \times 10^{-6} \text{ sec}^{-1}$ . Positive contours are solid, negative contours are dashed. Zero contour is annotated and is solid.

(a) The leading CPC vector for all the data sets.

(b) The second CPC vector for all the data sets.

Figure 12. Common Principal vectors for the 200 hPa monthly mean divergence for the four CSM 20 year data sets. Contour interval is  $1.0 \times 10^{-7} \text{ sec}^{-1}$ . Positive contours are solid, negative contours are dashed. Zero contour is annotated and is solid.

- (a) Leading CPC vector for all four data sets.
- (b) The second CPC vector for all four data sets.

Figure 13. Common Principal vectors for the 200 hPa monthly mean divergence for two 20 year sections of the NCEP/NCAR reanalysis. Contour interval is  $1.0 \times 10^{-7} \text{ sec}^{-1}$ . Positive contours are solid, negative contours are dashed. Zero contour is annotated and is solid.

- (a) Leading CPC vector for both data sets.
- (b) The second CPC vector for both data sets.